Computers and Chemical Engineering 104 (2017) 185–200

Contents lists available at ScienceDirect

Computers and Chemical Engineering

journal homepage: www.elsevier.com/locate/compchemeng

Temperature balancing in steam methane reforming furnace via an integrated CFD/data-based optimization approach

Anh Tran [a], Andres Aguirre [a], Marquis Crose [a], Helen Durand [a], Panagiotis D. Christofides [a,b,*]

[a] Department of Chemical and Biomolecular Engineering, University of California, Los Angeles, CA 90095-1592, USA
[b] Department of Electrical Engineering, University of California, Los Angeles, CA 90095-1592, USA

ARTICLE INFO

Article history:
Received 30 January 2017
Received in revised form 9 March 2017
Accepted 11 April 2017
Available online 25 April 2017

Keywords:
Methane reforming
Furnace-balancing
Process operation
Process optimization
Data-based modeling
Valve defects

ABSTRACT

In this work, we introduce a furnace-balancing scheme that generates an optimal furnace-side feed distribution that has the potential to improve the thermal efficiency of a reformer. The furnace-balancing scheme is composed of four major components: data generation, model identification, a model-based furnace-balancing optimizer and a termination checker. Initially, a computational fluid dynamics (CFD) model of an industrial-scale reformer, developed in our previous work, is used for the data generation as the model has been confirmed to simulate the typical transport and chemical reaction phenomena observed during reformer operation, and the CFD simulation data is in good agreement with various sources in literature. Then, we propose a model identification process in which the algorithm is formulated based on the least squares regression method, basic knowledge of radiative heat transfer and the existing furnace-side flow pattern. Subsequently, we propose a model-based furnace-balancing optimizer that is formulated as an optimization problem within which the valve position distribution is the decision variable, and minimizing the sum of the weighted squared deviations of the outer reforming tube wall temperatures from a set-point value for all reforming tubes with a penalty term on the deviation of the valve positions from their fully open positions is the objective function. CFD simulation results provide evidence that the optimized furnace-side feed distribution created by the furnace-balancing scheme can reduce the severity of nonuniformity in the spatial distribution of furnace-side temperature in the combustion chamber even when the reformer is under the influence of common valve-related disturbances.

1. Introduction

Hydrogen is a key material for the petroleum and fine chemical manufacturing industries. In petroleum refineries, many refining catalytic processes (e.g., the hydrotreating process, hydrocracking process and hydrodesulfurization process) consume hydrogen. Specifically, the hydrotreating process uses hydrogen to convert olefins to paraffins, and the hydrocracking process uses hydrogen to cleave sigma carbon-carbon bonds; these refining processes serve the same purpose of increasing the hydrogen to carbon ratio in the downstream process reactants, allowing these downstream processes to have higher efficiency. Additionally, the hydro-desulfurization process uses hydrogen to remove thiol compounds from the raw natural gas feedstock to prevent the catalysts of downstream processes from being deactivated. In the fine chemical manufacturing industries, hydrogen is the main component of synthesis gas; e.g., in the production of ammonia, hydrogen is reacted with nitrogen in a 3:1 ratio. In the production of thin solar films, the feedstock to a plasma enhanced chemical vapor deposition reactor is typically composed of 90% hydrogen and 10% silane (Crose et al., 2017). Inside the reactor, the feedstock is converted into hydrogen and silane radicals, which are the major deposition species directly contributing to film growth. Moreover, hydrogen is also a clean and efficient energy carrier as hydrogen can be used to generate electrical energy in fuel cells.

In an industrial setting, the steam methane reforming (SMR) process accounts for ~48% of worldwide hydrogen production (Ewan and Allen, 2005). The SMR process is an endothermic process that converts methane and superheated steam into hydrogen and carbon oxides (carbon dioxide and carbon monoxide) in the presence of a nickel-based catalyst network. The process takes

* Corresponding author at: Department of Chemical and Biomolecular Engineering, University of California, Los Angeles, CA 90095-1592, USA.
E-mail address: pdc@seas.ucla.edu (P.D. Christofides).

http://dx.doi.org/10.1016/j.compchemeng.2017.04.013
0098-1354/

place inside a unit that consists of two closed domains. Typically, in one domain the fuel reacts with excess oxygen in air to generate the necessary thermal energy to drive the endothermic steam reforming of hydrocarbons taking place in the other domain. The core unit of the SMR process is the steam methane reformer, in which the two closed domains are referred to as the tube side and the furnace side. The tube side is defined as a collection of hundreds of tubular reforming reactors (which are referred to as reforming tubes), and the furnace side is defined by the remaining components of the reformer including the burners, combustion chamber and flue-gas tunnels. Reformers come in four typical configurations which are bottom-fired, terrace wall-fired, top-fired and side-fired reformers. The categorization of the reformer configurations is based on the locations of burners, which governs the temperature distribution inside the reformer and the thermal interaction between the two closed domains. Specifically, bottom-fired reformers are characterized by a constant heat flux along the reforming tubes (terrace wall-fired reformers are a modified version of the bottom-fired configuration) (Ferreira-Aparicio et al., 2005). Top-fired reformers generate a unique temperature distribution in the furnace side that allows a significant amount of heat to enter the tube side near the reforming tube inlets. Side-fired reformers allow flexible control of the temperature distribution inside the combustion chamber. In the steam methane reforming application, the key reactions of the SMR process are endothermic and reversible, and therefore, a reformer configuration that allows significant heat transfer to the tube side near the reforming tube entrance is an appropriate design, and motivated by this, the top-fired furnace configuration is the most frequently used reformer configuration in industry. The top-fired reformer of interest in the present work is typically used at fine chemical manufacturing plants that are designed to produce high purity hydrogen on a commercial scale.

A typical hydrogen plant consists of the SMR, heat recovery, water-gas-shift and purification processes (Kroschwitz and Howe-Grant, 1999). Specifically, as synthesis gas, which is the product of the SMR process, exits the reformer, it typically enters a system of heat recovery exchanger networks to produce additional superheated steam supply for the plant. Next, the cooled synthesis gas enters the water shift reactor in which carbon monoxide is oxidized to carbon dioxide, additional hydrogen is produced, and the overall methane conversion is increased. Subsequently, the synthesis gas undergoes a separation process to remove the unreacted steam prior to entering the pressure swing adsorption (PSA) unit in which hydrogen is separated from the byproducts and unreacted methane to produce the high purity hydrogen product. Among the major equipment at the hydrogen plant (i.e., the reformer, water shift reactor, heat exchanger network and PSA unit), the reformer is the largest and is the most energy intensive. Therefore, the efficiency of the hydrogen plant is determined by the thermal efficiency of the reformer.

The nominal operating condition of a reformer is typically calibrated with the goal of extending the reformer service life by adjusting (reducing) the hydrogen production rate of the plant. Specifically, the endothermic characteristics of the SMR process suggest that the reformer interior should be kept at high temperature to increase the thermal efficiency because a higher conversion of hydrogen can be accomplished by a higher outer reforming tube wall temperature (Lee et al., 2013). However, an increase in the outer reforming tube wall temperature of 20 K above the designed operating value can reduce the reforming tube expected service life of 100,000 h by half (Pantoleontos et al., 2012; Latham, 2008). In addition, when the outer reforming tube wall temperature exceeds the design value by a significant margin, the reforming tube wall might rupture, resulting in production and capital losses. It becomes evident that the reformer thermal efficiency is constrained by the design temperature of the reforming tube wall and, therefore, depends on the spatial distribution of the furnace-side temperature in the reformer. Specifically, a higher reformer thermal efficiency is observed with a more uniform temperature distribution in the combustion chamber (Kumar et al., 2015). On the other hand, the spatial distribution of the furnace-side temperature in the combustion chamber is linked to the outer reforming tube wall temperature (OTWT) distributions along the reforming tube length, each of which is defined as a collection of radially averaged outer wall temperatures of 336 reforming tubes at a fixed distance away from the reforming tube inlets and can be monitored by a system of infrared (IR) cameras situated around the reformer. Hence, OTWT distributions can be used to represent the spatial distribution of the furnace-side temperature, and indeed, uniform OTWT distributions along the reforming tube length (i.e., all reforming tubes have the same outer wall temperature profile) allow the reformer to be operated at the designed capacity (Dunn et al., 2002). In the present work, the degree of nonuniformity in the OTWT distribution is defined as the maximum variation in the radially averaged outer wall temperature between all reforming tubes in the reformer at a specified distance away from the reforming tube inlets (Zheng et al., 2010; Oprins and Heynderickx, 2003; Kumar et al., 2015). The existence of the nonuniformity in the OTWT distribution in reformers has been confirmed with experimental data recorded by a system of IR cameras (Zheng et al., 2010), and operating strategies designed to counter the high degree of nonuniformity in the OTWT distribution in the reformers has been of great interest to industry and has been frequently discussed in published literature. This is because when the degree of nonuniformity in the OTWT distribution inside the combustion chamber is severe, the reformer must be operated at suboptimal conditions in which the overall average outer wall temperature among all reforming tubes along their heated length is sufficiently smaller than the design value to compensate for the wide spread of the OTWT distribution. Hence, the hydrogen production rate of the reformer is less than the designed capacity of the reformer. Additionally, a reformer that possesses a high degree of nonuniformity in the OTWT distribution, which can be as severe as 110 K, is referred to as an imbalanced reformer, and an imbalanced reformer has noticeably lower radiative heat transfer efficiency compared to a balanced reformer (Kumar et al., 2015).

The major cause of the nonuniformity in the OTWT distribution is an asymmetric distribution of the velocity of the combustion product mixture in the furnace side that is commonly referred to as the furnace-side flow pattern on which the spatial distribution of the furnace-side temperature depends (Zheng et al., 2010). Specifically, Zheng et al. (2010) shows that a maldistribution of the furnace-side flow in the reformer can cause flame impingement, which creates local hot-spots along the reforming tube length and causes the OTWT distribution to have a higher degree of nonuniformity. The outer wall temperature at the hot-spots may significantly exceed the design temperature of the reforming tube walls, which reduces the reformer service life. The asymmetric furnace-side flow pattern is the result of having an asymmetric geometry for a reformer. For example, the reformer considered in this work, developed and validated in Tran et al. (2017) and shown in Fig. 2, is designed such that the furnace-side outlets of the combustion chamber are situated on the front side of the refractory wall. Hence, the asymmetric furnace-side flow pattern is an intrinsic characteristic of the reformer and cannot be resolved without having to redesign the reformer geometry and to rebuild the reformer. However, Oprins and Heynderickx (2003) demonstrates that the nonuniformity in the OTWT distribution under the influence of the asymmetric furnace-side flow pattern can be altered by redistributing the furnace-side feed for which the definition is provided in Section 2.1.

Motivated by the above considerations, the present work focuses on developing a model-based furnace-balancing scheme to determine an optimized furnace-side feed (FSF) distribution of the reformer such that OTWT distributions along the reforming tube length in the reformer have a reduced degree of nonuniformity. The concept of 'furnace-balancing' is well-founded, and in particular, Kumar et al. (2015, 2016) are noteworthy examples of many proofs of concept in literature, which address the problem of the optimized FSF distribution. Nevertheless, the features of the high fidelity reformer CFD model, model identification process and furnace-balancing optimizer clearly differentiate the present work from those in literature. The remainder of this manuscript is structured as follows: in Section 2, an overview of the model-based furnace-balancing scheme is presented, of which the algorithm of each component is detailed in Sections 2.1–2.4. In Section 2.1, the physical description, process modeling and process simulation of the high fidelity reformer CFD model are presented. Specifically, the reformer CFD model is created from a multiblock structured hexahedral reformer mesh with ~41 million grids that has a reasonably acceptable mesh quality, and the corresponding CFD data generated from the simulations of the reformer CFD model is verified to be mesh-independent. The modeling strategies of the reformer CFD model are selected from a pool of potential models such that the chosen models can simulate characteristics of the transport and chemical reaction phenomena observed inside the reformer during hydrogen production and require a reasonable computational resource. In addition, Tran et al. (2017) demonstrates that the CFD simulation data generated from the simulations of the reformer CFD model is in good agreement with various sources in the literature. In Section 2.2, the impact of the furnace-side flow pattern on the OTWT distributions along the reforming tubes is investigated, and the concept of a heating zone is introduced and is utilized to allow the model identification process to embed the characteristics of the reformer geometry and knowledge of the potential effects of the furnace-side flow pattern on the OTWT distribution into the data-driven model. The data-driven model derived from this 'hybrid' model identification process (i.e., a model identification strategy that uses information on the reformer geometry and effects of the furnace-side flow pattern on the OTWT distributions), which represents the reasonably accurate relationship between the OTWT distribution and the FSF distribution inside the reformer CFD model, can be obtained from a small set of CFD training data. This feature of the model identification process highlights contributions of the present work to the existing SMR modeling literature. In Section 2.3, the relationship between the FSF distribution and the flow control system of the reformer and the fundamental differences between properly functional and defective flow control valves (i.e., constituents of the flow control system) are presented. In Section 2.4, the algorithm of the furnace-balancing optimizer, of which the decision variables are the valve positions of the properly functional flow control valves, is presented. Then in Section 3.1, the proposed furnace-balancing scheme is deployed with the assumption that the reformer is properly functional, and the CFD data corresponding to the optimized FSF distribution generated by the proposed furnace-balancing scheme is used to evaluate its performance. Finally in Section 3.2, the proposed furnace-balancing scheme is deployed for the case in which the reformer is subjected to two different valve-related disturbances, and the CFD data corresponding to the reoptimized FSF distribution, generated by the proposed furnace-balancing scheme, is used to evaluate its ability to compensate for the additional constraints imposed by the disturbances.

2. Furnace-balancing scheme

The furnace-balancing scheme consists of four processes denoted by the rectangular boxes in Fig. 1 (i.e., data generation, model identification, a model-based furnace-balancing optimizer and a termination checker). It is designed to search for the optimized FSF distribution such that the nonuniformity in OTWT distributions along the reforming tubes and the overall maximum outer reforming tube wall temperature (i.e., the maximum radially averaged outer wall temperature among all reforming tubes along their heated length) are minimized, which facilitates the subsequent increase of the total FSF flow rate to the reformer to achieve higher production rates of hydrogen and superheated steam without shortening the reformer service life.

Ideally, the initial FSF distribution used by the furnace-balancing scheme is chosen to be the nominal FSF distribution of the online reformer at hydrogen manufacturing plants; however, the

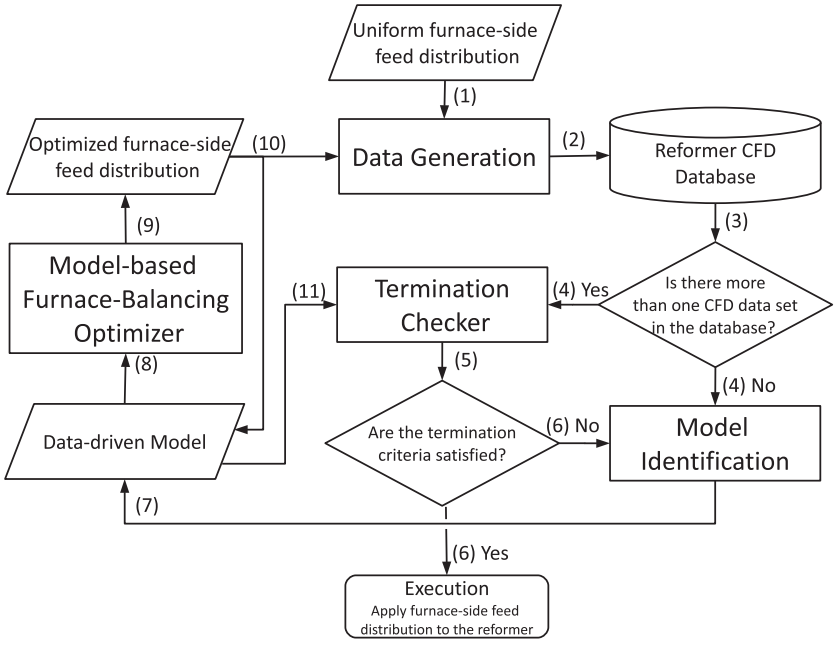

Fig. 1. Flowchart of the furnace-balancing scheme.

industrial data concerning reformer operational settings is limited, e.g., although the total FSF flow rate is available for public access, to the extent of our knowledge the FSF distribution of the reformer has never been reported. Additionally, it is evident that the OTWT distribution is dependent on the asymmetric furnace-side flow pattern as discussed in Section 1, and the quantitative relationship between them has not yet been revealed; therefore, we do not have sufficient information to form an educated initial guess of the optimized FSF distribution. As a result, the initial guess of the optimized FSF distribution is assumed to be a uniform distribution (i.e., the furnace-side feed is uniformly distributed among the inner-lane burners and among the outer-lane burners, and this distribution is referred to as the uniform FSF distribution.) Hence, the reformer CFD simulation result computed using the uniformly distributed furnace-side feed serves as a basis for this investigation. Initially, the uniform FSF distribution is implemented as the boundary condition of the reformer CFD model in the data generation process of Fig. 1. The corresponding CFD data generated from the simulation of the reformer CFD model is stored in the reformer CFD database (which is the Hoffman2 computing cluster at UCLA in this work). Subsequently, the CFD data in the reformer CFD database is used by the model identification process to derive a data-driven model, which is a single input/single output (SISO) model that quantifies the impact of the FSF distribution on the OTWT distribution. Next, the model-based furnace-balancing optimizer utilizes the data-driven model to predict the optimized FSF distribution such that the degree of nonuniformity in the OTWT distribution is minimized. Then, the optimized FSF distribution is re-applied as the boundary condition of the reformer CFD model in the data generation process and is also used as the input of the data-driven model to generate two sets of the optimized OTWT distributions. Thereafter, the termination checker process utilizes the corresponding two data sets to evaluate the accuracy of the data-driven model and the performance of the furnace-balancing scheme such that when the difference between the two data sets is within 1%, or when the performance of the furnace-balancing scheme is no longer improved, the termination checker process signals for the furnace-balancing scheme to be terminated and the last optimized FSF distribution to be applied to the on-line reformer. In the remainder of this section, the data generation, model identification and model-based furnace-balancing optimizer processes will be presented.

2.1. Data generation

The first step of the furnace-balancing scheme (i.e., the data generation process) utilizes a reformer CFD model developed in our previous work from which the CFD simulation data is generated and is consistent with various sources in the literature (Tran et al., 2017). The reformer CFD model is created based on an on-line top-fired steam methane reformer designed by Selas Fluid Processing Corporation (Latham, 2008).

The reformer has a width of ~16 m, length of ~16 m and height of ~13 m. This unit consists of 336 reforming tubes, 96 burners and 8 flue-gas tunnels as shown in Fig. 2. Inside the reformer, 336 reforming tubes are arranged as seven rows of 48 units inside which commercial nickel-based catalyst pellets are used as packing material. At the ceiling of the reformer, 96 burners are positioned as eight rows of 12 units. Among the 96 burners, there are 24 outer-lane burners which are adjacent to one row of 48 reforming tubes and 72 inner-lane burners which are adjacent to two rows of 48 reforming tubes. The outer-lane burners are designed to be smaller and to have lower maximum flow capacity compared to the inner-lane burners. At the floor of the reformer, eight flue-gas tunnels are placed parallel to the rows of reforming tubes. On each side of the flue-gas tunnels, there is a row of 35 evenly spaced rectangular extraction ports. The reformer produces 2,800,000 Nm^3 of high-purity hydrogen and 1,700,000 kg of superheated steam per day with an annual operating cost of 62,000,000 dollars.

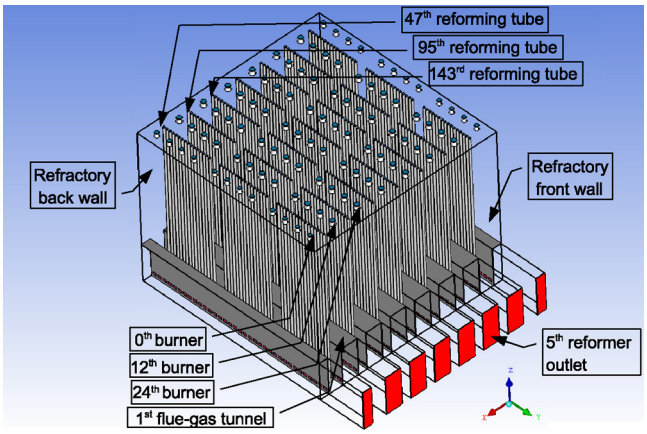

Fig. 2. The isometric view of an industrial-scale, top-fired, co-current reformer with 336 reforming tubes, which are represented by 336 slender cylinders, 96 burners, which are represented by 96 frustum cones, and 8 flue-gas tunnels, which are represented by 8 rectangular intrusions.

In CFD study, mesh generation is the most critical and time-consuming process because a CFD model created from a poor quality grid requires more computational resources and a longer computational time to calculate a converged simulation result, and the result is likely to carry a large numerical error (ANSYS Inc., 2013). The choice of meshing strategy (i.e., the structured multi-block hexahedral meshing) for creating the reformer mesh and the criteria (i.e., maximum orthogonal factor, minimum ortho skew, and maximum aspect ratio) for evaluating the reformer mesh quality are identical to those in Tran et al. (2017) and, therefore, will not be repeated for brevity. However, the current reformer mesh in this work is designed to be finer than that in Tran et al. (2017) (i.e., the total number of grids is increased from ~29 million to ~41 million) and to have significantly better mesh quality compared to the mesh in Tran et al. (2017) as shown in Table 1. Although the reformer CFD model built from the finer reformer mesh is expected to require a longer computational time than the reformer CFD model in Tran et al. (2017) with the computational resources that we have at our disposal (i.e., 80 cores on the Hoffman2 cluster), the CFD data generated by the current reformer CFD model is expected to be a more accurate representation of the experimental data. The increased accuracy resulting in the increased computational time is essential because the magnitude of the reduction in the overall maximum outer reforming tube wall temperature in a balanced reformer is expected to be small (if not negligible) compared to its typical value. It is important to note that though the current multiblock structured hexahedral reformer mesh with ~41 million grids has a minimum orthogonal factor of 0.459 and a maximum ortho skew of 0.541, which may not appear to be suitable when the accuracy of the CFD data is the primary interest, its average orthogonal factor of 0.964 and average ortho skew of 0.036 are nearly ideal, which dismiss the initial concern of the impact of the mesh quality of the CFD data accuracy.

Table 1
Reformer mesh quality.

	Current mesh	Mesh in Tran et al. (2017)	Recommended range
Number of grids (millions)	41	29	
Min orthogonal factor	0.459	0.181	0.167–1.000
Max ortho skew	0.541	0.819	0.000–0.850
Max aspect ratio	28.5	28.5	1–100

In our previous work (Lao et al., 2016; Tran et al., 2017), the modeling strategies of the reformer are chosen based on the transport and chemical reaction phenomena expected inside the reformer during hydrogen production and are selected to require a reasonably powerful computational resource and moderate computing time to create the reformer CFD model. In particular, the reformer CFD model is able to simulate the non-premixed combustion characteristics of the furnace-side fuel stream by using the standard k–ϵ turbulence model with the ANSYS enhanced wall treatment, finite rate/eddy dissipation (FR/ED) model and global volumetric kinetic models of methane/hydrogen combustion in air (Bane et al., 2010; Nicol, 1995); therefore, burners in the reformer CFD model are supplied with the well-mixed feed (i.e., the furnace-side feed), which is created by mixing the fuel stream and the combustion air stream. Additionally, the reformer CFD model is capable of simulating radiative heat transfer between the furnace-side flow, combustion chamber refractory walls and outer reforming tube walls by using an empirical correlation between the furnace-side radiative properties and temperature (Maximov, 2012), Lambert Beer's law, Kirchoff's law and the discrete ordinate method (ANSYS Inc., 2013). Furthermore, the reformer CFD model can simulate the SMR process in the tube side by means of the standard k–ϵ turbulence model, FR/ED model and global kinetic model of the SMR process (Xu and Froment, 1989). Moreover, the reformer CFD model can also simulate the effects of the catalyst network on the tube side flow by employing the ANSYS porous zone function for which the parameters are estimated from the semi-empirical Ergun equation and relevant typical industrial data (Lao et al., 2016).

In our previous work, it has been established that the simulation of the reformer CFD model is sensitive to initial guesses (e.g., when the simulation of the reformer CFD model is initialized by the ANSYS standard initialization based on the boundary conditions of the CFD model, it quickly diverges) (Tran et al., 2017). In Tran et al. (2017), a step-by-step converging strategy is proposed to counter the numerical instability issue and to accelerate the rate of convergence of the simulation, which reduces the computational time devoted to generate the converged CFD data. Hence, the converging strategy is again utilized in the present work to obtain the CFD data of the reformer CFD model in which the uniform FSF distribution is implemented as the boundary condition, and the CFD data is expected to be determined by the ANSYS Fluent parallel solver after ~3 days on the 80 private cores on UCLA's Hoffman2 Cluster. Although subsequent simulations of the reformer CFD model, in which the optimized FSF distribution is implemented as the boundary condition, could be executed with the converging strategy, we have found that we can further reduce the computational time to slightly more than a day by utilizing a CFD data set stored in the reformer CFD database as an initial guess for the simulations and executing with a two-step converging strategy. Specifically, the data generation process of each iteration of the furnace-balancing scheme begins with the simulation of the isothermal, non-reacting (INR) reformer CFD model (Tran et al., 2017), which is initialized based on the reformer CFD data and is solved by the aggressive mode of the ANSYS Fluent solver to generate an intermediate solution that contains information of the new flow fields (i.e., the velocity and turbulence fields of the furnace-side and tube-side flows) of the balanced reformer CFD model. This is because despite the differences in the composition and temperature fields of the furnace-side and tube-side flows computed by the INR reformer CFD model and the reformer CFD model, their furnace-side and tube-side flow fields are expected to be similar (ANSYS Inc., 2013; Vuthaluru and Vuthaluru, 2006; Tran et al., 2017). Finally, the simulation of the (complete) reformer CFD model is initialized based on the intermediate CFD data (which contains information of the new flow fields in addition to the temperature and species fields from the reformer CFD data of a prior iteration) and is solved by the aggressive mode of the ANSYS Fluent solver until the convergence criteria, which are adopted from (Tran et al., 2017) and described in the next paragraph, are met.

Typically, after the global normalized residuals of the conserved transport variables are on the order of 10^{-4}, the total mass flow rate integrated over all boundaries of the reformer CFD model is ~0 kg s^{-1}, the total heat transfer rate integrated over all boundaries of the reformer CFD model is less than 1% of the reformer total fired duty, and the absolute residuals of the temperature of the furnace-side flow at five different locations inside the combustion chamber are less than 1 K, the simulations would be terminated. In the present work, the simulations are continued because we recognize that the global normalized residuals are nonzero which indicates that the CFD data fluctuates around the true steady-state solution of the reformer CFD model, and therefore, the averaged CFD data of many converged CFD data sets is the most accurate representation of the reformer steady-state solution. In the effort of acquiring the more accurate CFD data for each reformer CFD model, the simulation is kept running for an additional 300 iterations, which correspond to ~5–10% of the total computational time, and the corresponding CFD data is periodically saved in the reformer CFD database every 100 iterations creating a total of four CFD data sets for each reformer CFD model, of which the average CFD data is utilized by subsequent processes of the furnace-balancing scheme. Although the effort to obtain the more accurate CFD data results in increased computational time, the trade-off is critical because the reduction in the maximum outer reforming tube wall temperature due to the optimized FSF distribution is expected to be substantially smaller than the overall average outer wall temperature of the reforming tubes.

2.2. Model identification

The second step of the furnace-balancing scheme (i.e., the model identification process) utilizes the cumulative reformer CFD database collected from the data generation process to derive a data-driven model describing the relationship between the OTWT distribution at a specified distance away from the reforming tube inlets and the FSF distribution. In the present work, we have found that the relationship can be assumed to be linear, and the data-driven model can still provide a reasonably accurate prediction of the OTWT distribution, which is generated by the reformer CFD model, given a sufficiently large reformer CFD database. Therefore, the radially averaged outer reforming tube wall temperature of the ith reforming tube at the fixed distance away from the reforming tube inlet (T_i (K)), which is an element of the OTWT distribution, can be approximated by a linear combination of the FSF flow rates of all 96 burners (i.e., the FSF distribution) as follows,

$$T_i = \sum_{j=0}^{95} \alpha_{ij} F_j \tag{1}$$

where F_j (kg s^{-1}) is the furnace-side feed flow rate of the jth burner and α_{ij} (K kg^{-1} s) is the empirical coefficient of the data-driven correlation corresponding to the ith reforming tube and jth burner, which is to be determined by the model identification process. In this study, the outer-lane/inner-lane burners and reforming tubes are indexed from 0th to 95th and 0th to 335th in the specified patterns as shown in Fig. 2. As a result, the model identification process created based on our assumption of the linear relationship between the OTWT and FSF distributions is an optimization problem with 32,256 decision variables. Due the sheer number of decision variables, the model identification process is expected to be a computationally expensive algorithm. Hence, in the remainder of this section, the concept of a heating zone is introduced

in an effort to decrease the computational time for deriving the data-driven model, and a modified formulation of the model identification process is presented.

In high-temperature applications, thermal radiation is the dominant mode of heat transfer, and the reformers are commonly referred to as radiant heat exchangers (Kumar et al., 2015). Olivieri and Vegliò (2008) shows that radiative heat transfer accounts for ~95% of the total heat transfer in the top-fired reformer investigated in that work, which suggests that the OTWT distribution is primarily controlled by thermal radiation. This is because the rate of energy transferred by thermal radiation between two blackbodies at different temperatures is commonly modeled as being proportional to the difference in temperatures raised to the fourth power (i.e., $\Delta(T^4)$), while the rate of heat transfer by conduction and convection between them is proportional to the temperature difference (i.e., $\Delta(T)$). However, the rate of heat transfer by thermal radiation decreases drastically with increasing distance between two blackbodies because it is proportional to the radiation intensity, which is inversely proportional to the distance between the two blackbodies raised to the second power. This idea allows us to assume that when the distance between a specified burner and reforming tube is sufficiently large, the furnace-side feed flow rate of the burner has negligible impact on the average outer reforming tube wall temperature. In this study, the distance between a specified burner and reforming tube is defined as the distance between the projection of the burner centroid and the projection of the reforming tube centroid onto any 2-D horizontal cross-sectional plane. To quantitatively determine the local radiative heating effect on the OTWT distribution due to the furnace-side feed flow rate of each burner, we consider the following simplifying assumptions: each burner creates a heating zone represented by a blue cylindrical volume as shown in Fig. 5, the heating zones of the burners have an identical size and shape, and the FSF flow rate of the jth burner only affects the average outer wall temperature values of the reforming tubes which are located inside the heating zone of the jth burner.

On the other hand, it has been established that the furnace-side flow pattern can influence the OTWT distribution, e.g., a maldistribution of the furnace-side flow pattern in the reformer can potentially cause flame impingement, which might make the outer wall temperature values of some reforming tubes exceed the design temperature, causing the OTWT distribution to have a higher degree of nonuniformity as discussed in Section 1. Hence, it is desired that the model identification process can create a data-driven model that is also capable of accounting for the effect of the furnace-side flow pattern on the OTWT distribution. We begin by utilizing the existing reformer CFD data reported in Tran et al. (2017) to construct the velocity vector fields of the furnace-side flow pattern as shown in Fig. 3, which allows us to form a hypothesis regarding the underlying mechanism by which the furnace-side flow field affects the OTWT distribution. Specifically, Fig. 3 indicates that the hot combustion products (i.e., the furnace-side flow) enter the flue-gas tunnels through the extraction ports and move toward the reformer outlets. The existing furnace-side flow pattern appears to cause the wall temperature of the flue-gas tunnels to increase with decreasing distance toward the reformer outlets as shown in Fig. 4. Additionally, Fig. 4 shows that the minimum wall temperature of the flue-gas tunnel of 1240 K is greater than the maximum temperature of the reforming tube wall of 1183 K (Tran et al., 2017), so it is reasonable to assume that the reforming tubes might receive additional radiative heating from the neighboring flue-gas tunnels. However, the magnitude of the additional heating transferred to each reforming tube from the neighboring flue-gas tunnels depends on the location of the reforming tube with respect to the reformer outlets. Particularly, because the flue-gas tunnels are at higher temperature toward the reformer outlets, the reforming tubes that are situated closer to the reformer outlets are

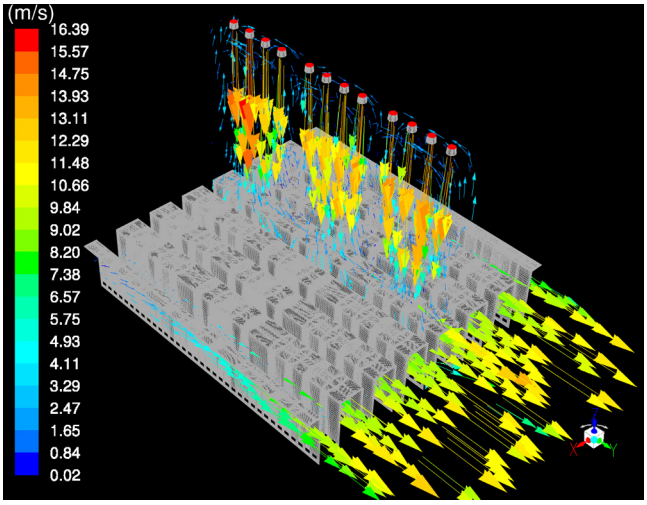

Fig. 3. The velocity vector field of the furnace-side flow pattern in the vicinity of the 4th burner row in the reformer is constructed from the reformer CFD data (Tran et al., 2017). The outlets of the reformer are situated at the bottom right corner and are placed in the direction of the velocity vectors inside the flue-gas tunnels.

expected to receive higher amounts of additional radiative heating from the neighboring flue-gas tunnels. It is important to note that the existing furnace-side flow pattern (Fig. 3) also suggests that the additional radiative heating received by the reforming tubes that are situated near the reformer outlets can be from the combustion products of the burner that is situated near the reformer back wall. The analysis motivates us to develop heating zones with the shape shown in Fig. 5 in the effort of making the data-driven model aware of the furnace-side flow pattern and its effects on the OTWT distribution. It is important to note that when a larger cylindrical heating zone is utilized in the model identification process, each burner is assumed to influence more surrounding reforming tubes in addition to those that are situated in the direction toward the reformer outlets and in the two adjacent rows of reforming tubes, which may allow the data-driven model to be more accurate with respect to the reformer CFD data at the cost of increased computational time. We conducted a study with various dimensions of the burner heating zone to determine the appropriate dimension of the cylindrical volume (i.e., r_{cyl}), and we have found that at $r_{cyl} \sim 3.4$ m,

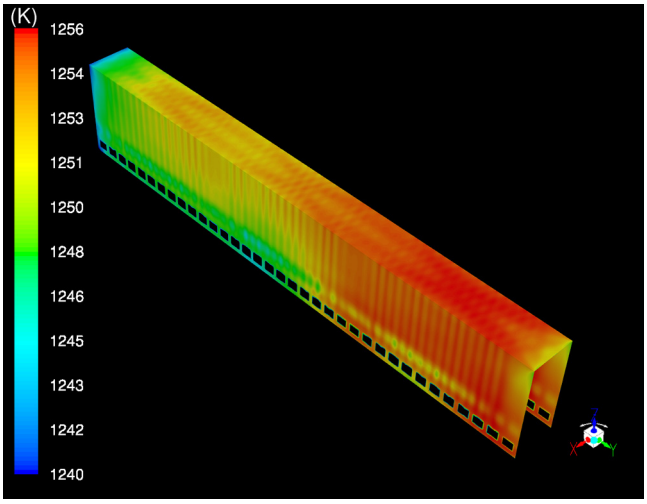

Fig. 4. The temperature contour map of the 4th flue-gas tunnel, which is situated directly under the 4th burner row in the reformer, is shown. This contour map is created from the reformer CFD data in Tran et al. (2017). In Fig. 4, the outlets of the reformer are situated at the bottom right corner.

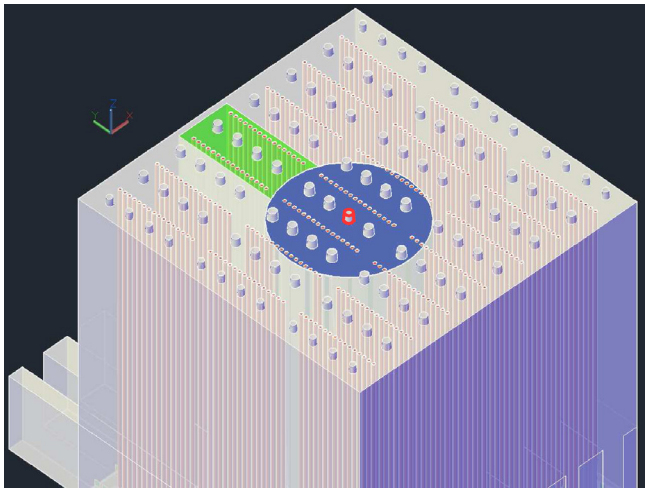

Fig. 5. A representation of a burner heating zone which is created by the highlighted burner in red. The burner heating zones are displayed by a blue cylindrical volume (where the reforming tubes are heated via thermal radiation from the furnace-side flow) and a green rectangular volume (where the reforming tubes are heated via thermal radiation from the neighboring flue-gas tunnels). It is assumed that only the reforming tubes located within the burner heating zones have the outer wall temperature values dependent on the FSF flow rate of the burner. (For interpretation of the references to color in this figure legend, the reader is referred to the web version of this article.)

we are able to form 336 sets of the tube-burner relationships, which are denoted by S_i and $i \in [0, 335]$ such that S_i contains the FSF flow rates of the burners on which the outer wall temperature of the ith reforming tube depends. The tube-burner relationships reduce the number of decision variables of the model identification algorithm from 32,256 to 6865 and, thus, allow the data-driven model to be created within a reasonable computing time interval.

The data-driven model is designed to account for the reformer geometry characteristics (i.e., the burner and reforming tube arrangements) and is designed to have the potential to account for the influence of the furnace-side flow pattern on the OTWT distribution by using the concept of a heating zone. The data-driven model utilizes a given FSF distribution to predict an OTWT distribution that is close to that taken from a reformer CFD simulation result in the least squares sense. The model identification process based on n sets of the reformer CFD data taken from the reformer CFD database is formulated as follows,

$$\min_{\alpha_{ij} \in [0,\infty)} \sum_{m=0}^{n-1} \left(\sum_{k=0}^{335} (T_{k,m} - T_{k,m}^{est})^2 \right)^2 \tag{2}$$

subject to

$$T_{k,m}^{est} = \sum_{j=0}^{95} \alpha_{kj} F_{j,m} \tag{3a}$$

$$\alpha_{kj} = 0 \qquad \text{if} \quad F_{j,m} \notin S_k \tag{3b}$$

$$\alpha_{kj} = \alpha_{ki} \qquad \text{if} \quad F_{j,m}, F_{i,m} \in S_k \quad \text{and} \quad d_{kj} = d_{ki} \tag{3c}$$

$$\left(\frac{d_{kj}}{d_{ki}} \right)^{\beta} \cdot \alpha_{kj} \geq \alpha_{ki} \geq \alpha_{kj} \quad \text{if} \quad F_{j,m}, F_{i,m} \in S_k \quad \text{and} \quad d_{kj} > d_{ki} \tag{3d}$$

where $T_{k,m}$ and $T_{k,m}^{est}$ are the average outer wall temperature of the kth reforming tube taken from the mth reformer CFD data set and the corresponding value generated by the data-driven model given the mth furnace-side feed distribution as shown in Eq. (3a), respectively, $F_{j,m}$ is the furnace-side feed flow rate of the jth burner derived from the mth reformer CFD data set, $\beta = 4.0$ is an empirical constant of the data-driven model estimated from the study of the burner heating zone, d_{kj} is the distance between the kth reforming tube and the jth burner and d_{ki} is the distance between the kth reforming tube and the ith burner. In Eqs. (3a)–(3d), the ranges of k, i, j and m are 0–335, 0–95, 0–95 and 0–n, respectively. The cost function (Eq. (2)) of the model identification penalizes the deviation of the average outer wall temperature of each reforming tube generated by the data-driven model from that derived from the corresponding reformer CFD data set. Specifically, Eq. (3b) suggests that if the kth reforming tube is not situated within the heating zone of the jth burner ($T_{k,m} \neq T_{k,m}(F_{j,m})$), the data-driven model will assume that the furnace-side feed flow rate of the jth burner does not affect the kth outer reforming tube wall temperature. Additionally, Eq. (3c) indicates that if the distance between the kth reforming tube and the jth burner is equal to that between the kth reforming tube and the ith burner, the data-driven model then presumes that the effects of the burners on the kth outer reforming tube wall temperature are the same. Similarly, Eq. (3d) shows that if the distance between the kth reforming tube and the jth burner is greater than that between the kth reforming tube and the ith burner, the data-driven model then infers that the effects of the jth burner on the kth outer reforming tube wall temperature are weaker than those of the ith burner.

2.3. Valves and flow rate relation

Although the FSF distribution is used as the boundary condition of the high fidelity reformer CFD model and is chosen as the input of the data-driven model, it cannot be directly controlled and is not typically measured in industrial practice. Indeed, the FSF distribution is controlled by a system of flow regulators consisting of a finite number of flow control valves. Specifically, because the burners in the reformer are interconnected, a fractional amount of the FSF flow rate of the jth burner can be redistributed to other units by partially closing the corresponding flow control valve. This suggests that the optimized FSF distribution can be produced by appropriately adjusting the percent open positions of all flow control valves in the flow regulator system, which is referred to as the valve position distribution. Hence, the merit of the high fidelity reformer CFD model and of the data-driven model for the furnace-balancing application, which aims to reduce the degree of the temperature nonuniformity in the combustion chamber and to increase the reformer thermal efficiency, is evident.

In an industrial setting of commercial-scale hydrogen production, the furnace-side feed flow rate of a burner in the reformer may not be individually regulated. In the present work, we assume that every set of two consecutive burners in a row of twelve burners is controlled by a flow control valve, and therefore, it is also reasonable to assume that the same FSF flow rate is delivered to these burners. Additionally, we assume that the FSF distribution is regulated by two distinct linear flow control valve models with different maximum capacities. Among the flow control valve models, one valve model with a larger maximum capacity is used for the inner-lane burners, and the other valve model with a smaller maximum capacity is implemented in the outer-lane burners such that when valves are at the same opening position, the FSF flow rate of the outer-lane burners is 60% of that of the inner-lane burners. Based on the burner arrangement in the reformer and the capacity ratio of the inner-lane valve model and the outer-lane valve model, the valve-position-to-flow-rate converter is formulated as follows,

$$[F] = \delta \cdot [X] \cdot [Y] \cdot [V] \tag{4}$$

subject to

$$[V] \in R^{48 \times 1} \tag{5a}$$

$$[X] \in R^{96\times 96} X_{ij} = 0.6; \quad i = j \quad \text{where} \quad i \in [0, 11] \cup [84, 95]$$
$$X_{ij} = 1.0; \quad i = j \quad \text{where} \quad i \in [12, 93] \tag{5b}$$
$$X_{ij} = 0.0; \quad i \neq j$$
$$[Y] \in R^{96\times 48}$$
$$Y_{ij} = 1.0; \quad i = 2j \cup i = 2j+1 \quad \text{where} \quad j \in [0, 47] \tag{5c}$$
$$Y_{ij} = 0.0; \quad i \neq 2j \cap i \neq 2j+1 \quad \text{where} \quad j \in [0, 47]$$
$$[F] \in R^{96\times 1} \quad F_i \geq 0 \quad \forall i \in [0, 95] \tag{5d}$$
$$\delta = \frac{F_{tot}}{\|[X]\cdot[Y]\cdot[V]\|_1} \tag{5e}$$

where F_{tot} ($\mathrm{kg\,s^{-1}}$) is the total mass flow rate of the furnace-side feed to the reformer, δ is the valve-to-flow-rate proportionality coefficient and is dependent on the valve position distribution, $[F]$ is a vector of the FSF flow rate through each burner (the FSF distribution), $[X]$ is a transformation matrix that identifies the types of the flow control valves (i.e., the inner-lane and outer-lane valves) in the reformer, $[Y]$ is a transformation matrix that describes the burner arrangement in the reformer and $[V]$ is a vector of valve positions (the valve position distribution). A characteristic of the valve-to-flow-rate converter is that a FSF distribution can be produced by different valve position distributions by changing the inlet pressure of the furnace-side feed to the reformer. To illustrate this idea, we utilize a fictitious simplified interconnected flow system which consists of four inner-lane burners and is supplied with the constant total FSF mass flow rate of 4.0 ($\mathrm{kg\,s^{-1}}$). When both flow control valves regulating the four inner-lane burners are at 100% open, the total FSF flow rate to the simplified interconnected flow system is evenly distributed, i.e., the FSF flow rate to each inner-lane burner is expected to be 1.0 ($\mathrm{kg\,s^{-1}}$). When both flow control valves regulating the four inner-lane burners are 80% open, the FSF flow rate to each inner-lane burner is still required to be 1.0 ($\mathrm{kg\,s^{-1}}$) to maintain the constant total FSF mass flow rate of 4.0 ($\mathrm{kg\,s^{-1}}$) because of the two following reasons: the FSF flow rates of the two inner-lane flow control valves that are at the same valve position are equal, and the FSF flow rates of the two inner-lane burners that are regulated by a flow control valve are also assumed to be equal. The primary difference between the two case studies is in plant's efficiency, as the magnitude of the inlet pressure of the furnace-side feed to the reformer is expected to be higher in the second case study, which corresponds to a higher energy input to the compressor system leading to an increase in the operating cost of the reformer and a reduction in the plant's efficiency.

In the reformer, the flow control system has 48 flow control valves among which 36 valves are designated to regulate the FSF flow rates of the 72 inner-lane burners, and the valve position of each flow control valve must be adjusted to create the optimized FSF distribution. Therefore, the reformer thermal efficiency becomes susceptible to common valve-related problems (e.g., valve stickiness) as these disturbances prevent the valve position distribution that is designed to produce the optimized FSF distribution from being implemented. In this study, when a flow control valve is said to become defective, we assume that the flow control valve becomes stuck, and hence, the valve position cannot be adjusted, which prevents the furnace-side feed from being distributed according to the optimized distribution.

2.4. Model-based furnace-balancing optimizer

The third step of the furnace-balancing scheme (i.e., the model-based furnace-balancing optimizer) utilizes the data-driven model (Eq. (10b)) and the valve-position-to-flow-rate converter (Eq. (10a)) to derive an optimized FSF distribution that aims to reduce the degree of nonuniformity in the OTWT distribution. The furnace-balancing optimizer is designed as a multivariable optimization problem in which the decision variables are the positions of the properly functional flow control valves. Additionally, the furnace-balancing optimizer is designed to handle defective valves in the flow control system by adjusting the number of decision variables. For instance, if a flow control valve of the 0th and 1st outer-lane burners becomes defective, there are 47 functional valves in the flow control system, and therefore, the number of decision variables decreases from 48 (which corresponds to the total number of flow control valves in the reformer) to 47. During the initialization of the furnace-balancing optimizer, a text file documenting the current status of the flow control valves is provided, based on which the furnace-balancing optimizer identifies the defective valve(s) and the corresponding stuck valve position(s) to determine the number of decision variables.

The decision variables of the furnace-balancing optimizer are subjected to the practical constraint of the flow control valves (i.e., Eq. (10f), which is enforced to avoid extinguishing the flame) and the physical constraint of the flow control valves (i.e., Eq. (10e)). In addition, we assume that the total furnace-side feed derived based on typical industrial data is kept constant at F_{tot} (i.e., Eq. (10c)), when the optimized FSF distribution is computed. This strictly controlled operating window of the reformer allows the radial average temperature of the ith reforming tube at a fixed distance away from the reforming tube inlet to be expressed as a linear combination of the FSF distribution as shown in Eq. (10b).

In the development of the furnace-balancing optimizer, careful consideration regarding the characteristic of the valve-to-flow-rate converter must be given. Specifically, the valve-to-flow-rate converter allows a FSF distribution to be produced by different valve position distributions between which the primary difference is in the plant's efficiency because the valve position distribution deviates further away from the default distribution (i.e., in which flow control valves are fully open) and thus requires a higher inlet pressure of the furnace-side feed to the reformer leading to a higher energy input to the compressor system, an increase in the operating cost of the reformer and a reduction in the plant's efficiency. In the present work, a quantitative assessment of the deviation of a valve position distribution ($[V]$) from the default distribution ($[V]_0$) is computed as the 1-norm of the difference between $[V]_0$ and $[V]$, i.e., $\|[V]_0 - [V]\|_1$. Therefore, the furnace-balancing optimizer is designed to minimize the degree of nonuniformity in the OTWT distribution in a manner that requires the least duty of the compressor system to maximize the plant's efficiency and reformer service life by penalizing the weighted quadratic deviation of the outer wall temperature values of all reforming tubes from the set-point temperature (T_{AVE}),

$$\sum_{k=0}^{335} w_k (T_{AVE} - T_k^{est})^2, \tag{6}$$

and also penalizing the deviation of the optimized valve position distribution ($[V]$) from $[V]_0$,

$$\|[V]_0 - [V]\|_1 = \sum_{i=0}^{47} (V_{i,\max} - V_i). \tag{7}$$

The objective function of the furnace-balancing optimizer must signify that minimizing the degree of nonuniformity in the OTWT distribution has by far the highest priority and should not be compromised by the benefit of minimizing the duty of the compressor system. This idea is translated into mathematical expression of the penalty associated with the task of minimizing the compressor duty in the objective function of the furnace-balancing optimizer by normalizing the deviation of the optimized valve position distribution

from $[V]_0$, which is subsequently scaled by multiplying with the product of the penalty associated with the task of minimizing the degree of nonuniformity in the OTWT distribution and a weighting factor (γ),

$$\gamma \cdot \sum_{k=0}^{335} w_k (T_{AVE} - T_k^{est})^2 \cdot \frac{\sum_{i=0}^{47}(V_{i,\max} - V_i)}{\sum_{i=0}^{47}(V_{i,\max} - V_{i,\min})}. \quad (8)$$

As a result, the objective function of the furnace-balancing optimizer is formulated as shown in Eq. (9), in which the first term represents the penalty associated with the task of minimizing the degree of nonuniformity in the OTWT distribution, and the second term represents the penalty associated with the task of minimizing the compressor duty. The set-point temperature (T_{AVE}) can be computed based on the OTWT distribution from any of the previous CFD data sets from the reformer CFD database as shown in Eq. (10d) because the overall average outer wall temperature at the fixed distance away from the reforming tube inlets is expected to be constant despite the degree of nonuniformity in the OTWT distribution. Additionally, the initial guesses for the decision variables of the furnace-balancing optimizer are set to be 100% open (i.e., when the penalty on the control action is minimized) to allow the furnace-balancing optimizer to initially shift the focus on minimizing the degree of nonuniformity in the OTWT distribution and to avoid being stuck, which could happen when it is initially forced to accomplish both objectives simultaneously. The model-based furnace-balancing optimizer is formulated as follows,

$$\min_{\substack{V_j \in [60,100] \\ j=\{0,\ldots,47\}\backslash V_{def}}} \sum_{k=0}^{335} w_k (T_{AVE} - T_k^{est})^2 + \gamma \sum_{k=0}^{335} w_k (T_{AVE} - T_k^{est})^2 \cdot \frac{\sum_{i=0}^{47}(V_{i,\max} - V_i)}{\sum_{i=0}^{47}(V_{i,\max} - V_{i,\min})} \quad (9)$$

subject to

$$[F] = \delta \cdot [X] \cdot [Y] \cdot [V] \quad (10a)$$

$$T_k^{est} = \sum_{j=0}^{95} \alpha_{kj} F_j \qquad \forall \ F_j \in [F] \quad (10b)$$

$$\sum_{j=0}^{95} F_j = F_{tot}, \quad j = \{0,\ldots,95\} \quad (10c)$$

$$T_{AVE} = \frac{1}{336} \sum_{k=0}^{335} T_{k,m} \quad (10d)$$

$$V_{i,\max} = 100\% \qquad i = \{0,\ldots,47\} \quad (10e)$$

$$V_{i,\min} = 60\% \qquad i = \{0,\ldots,47\} \quad (10f)$$

$$V_{i,\min} \le V_i \le V_{i,\max} \qquad i = \{0,\ldots,47\}\backslash V_{def} \quad (10g)$$

where V_{def} is the set of indices of defective control valves (the notation $x\backslash y$ denotes that the components of the set x are considered except those that are also in set y), w_k is the weighting factor of the kth reforming tube (which is used to compute the penalty associated with the deviation of the predicted outer wall temperature of the kth reforming tube (T_k^{est}) from T_{AVE}), γ is the weighting factor of the penalty associated with the control action, V_i (the ith component of $[V]$) is the valve position of the ith flow control valve (which regulates the FSF flow rates of the $(2i)$th and $(2i+1)$th burners) and F_j (the jth component of $[F]$) is the optimized FSF flow rate of the jth burner. The idea of assigning the deviations of T_k^{est} from T_{AVE} of the reforming tubes different weights in the penalty associated with the degree of nonuniformity in the OTWT distribution is motivated by the fact that the local environments of the reforming tubes are not all identical, and specifically, the additional radiative heating provided for the reforming tubes from the neighboring flue-gas tunnels is expected to decrease with increasing distance away from the reformer outlets. Hence, we want to compensate for the nonuniform additional radiative heating along the rows of 48 reforming tubes by giving the most weight to the offsets of the reforming tubes that are the furthest away from the reformer outlets (e.g., the 47th reforming tube). Specifically, w_k is designed to monotonically decrease with the position (p_k) of the kth reforming tube in a row of 48 reforming tubes as follows,

$$p_k = k - 48 \cdot \left\lfloor \frac{k}{48} \right\rfloor \quad k \in \{0, 1, \ldots, 335\} \quad (11a)$$

$$w_k = w_k^{\max} \cdot \exp[-\beta_w \cdot (47 - p_k)] \quad p_k \in \{0, 1, \ldots, 47\} \quad (11b)$$

where $\lfloor \cdot \rfloor$ represents the 'floor' operator, and $w_k^{\max}$ and β_w are the parameters of w_k. These weights, combined with the form of the heating zones for the data-driven model discussed in Section 2.2, allow the furnace-balancing optimizer to account to some extent for the reformer geometry, furnace-side flow pattern and its potential influence on the OTWT distribution. Therefore, the furnace-balancing optimizer is expected to realize that the burners situated near the refractory back wall might have long range effects on the outer wall temperature of the reforming tubes near the reformer outlets. As a result, the optimized FSF distribution is expected to lessen the degree of nonuniformity in the OTWT distributions along the reforming tubes and to reduce the overall maximum temperature of the outer reforming tube wall, which creates room for improving the thermal efficiency of the reformer. It is important to note that $w_k^{\max} = 10.0$, $\beta_w = 0.05$ and $\gamma = 0.1$ are determined based on a trial-and-error approach until the largest reduction in the degree of nonuniformity in the predicted OTWT distribution is observed.

3. Simulation results

In this section, the average of four CFD data sets produced by the reformer CFD model, in which the uniform FSF distribution is used as the boundary condition, is utilized to analyze the existing degree of nonuniformity in OTWT distributions at different locations along the reforming tube length as shown in Table 2. We note that the spread of the OTWT distributions only raises our concerns about the reformer life service when the average temperature of the OTWT distribution at a fixed distance away from the reforming tube inlets is in the regime of the maximum value of average temperatures of the OTWT distributions along the reforming tube length. This is because if the average temperature of the OTWT distribution is high, the radially averaged maximum temperature for some tubes is likely to exceed the design temperature of the reforming tube wall, and therefore, the service life of the reformer is shortened. Additionally, Kumar et al. (2015) shows that OTWT distributions along the reforming tube length and the spatial distribution of the furnace-side temperature can be made to become more uniform by reducing the degree of nonuniformity in just one OTWT distribution. In the remainder of this section, we focus on the OTWT distribution that is ~6.5 m away from the reforming tube inlets as it has a relatively high overall average temperature (1165.08 K, which is ~99% of the maximum value in the average outer wall temperature profile), temperature range (67.7 K) and standard deviation (9.7 K). Only the OTWT distributions and the corresponding FSF distributions are utilized by the model identification to create the data-driven model as discussed in Section 2.2. Next, the model-based furnace-balancing optimizer

Table 2
OTWT distribution obtained from the reformer CFD model in which the uniform FSF distribution is used as the boundary condition.

Distance down reforming tubes (m)	T_{AVE} (K)	T_{Max} (K)	T_{Min} (K)	Standard deviation (K)
1.0	971.9	998.7	948.3	10.8
2.0	1035.3	1064.3	1010.8	11.6
3.0	1086.0	1114.6	1052.1	11.5
4.0	1123.2	1150.1	1076.5	11.7
5.0	1149.4	1172.7	1097.1	11.2
6.0	1161.6	1179.6	1110.6	10.1
6.5	1165.1	1183.2	1115.5	9.7
7.0	1168.5	1186.5	1121.1	9.3
8.0	1174.0	1192.3	1130.5	8.8
9.0	1179.3	1197.2	1138.1	8.0
10.0	1168.8	1187.6	1128.7	7.9
11.0	1164.1	1183.4	1125.0	8.1
12.0	1162.5	1181.7	1124.6	8.2

uses the status of the flow control system, the valve-position-to-flow-rate converter and the most up-to-date data-driven model to search for the optimized FSF distribution to minimize the degree of nonuniformity in the OTWT distribution. We note that each data set utilized by the model identification process requires 3.64×10^{-4} GB of storage space, while the original reformer CFD data, from which the OTWT distribution and FSF distribution are extracted, requires 112 GB of storage space, and therefore, the data-driven model might not be able to precisely predict the behavior of the reformer when the training data set is not sufficiently large. Hence, once an optimized FSF distribution is obtained from the furnace-balancing optimizer, the optimized FSF distribution is simultaneously used as the boundary condition of the reformer CFD and as the input of the data-driven model, and the corresponding data is utilized in the termination checker process, in which the accuracy of the data-driven model and the performance of the furnace-balancing scheme are evaluated. In the present work, the performance of the furnace-balancing scheme is assessed based on the percent reduction in the standard deviation of the OTWT distribution generated by the reformer CFD model, in which the optimized FSF distribution is used as the boundary condition, compared to that generated by the reformer CFD model, in which the uniform FSF distribution is used as the boundary condition.

Each iteration of the proposed furnace-balancing scheme solved by Ipopt (Wächter and Biegler, 2006) generates an optimized FSF distribution and quantitatively estimates the reduction of the degree of nonuniformity of the OTWT distribution within 30 h using 80 cores of the UCLA Hoffman2 Cluster, and ~90% of the computational time is designated to the data generation process. The termination checker process triggers a terminating signal after six iterations of the furnace-balancing scheme. It is worth noting that subsequent attempts to reoptimize the FSF distribution to compensate for the influences of common valve-related problems can be accomplished after fewer iterations of the furnace-balancing scheme as the data-driven model derived using the entire reformer CFD database is expected to accurately predict the reformer behavior.

Remark 1. It is the most beneficial for hydrogen plants to operate the reformer with the optimized FSF distribution such that the rate of hydrogen production and reformer service life is maximized. Hence, it would be illogical to frequently adjust the FSF distribution in the absence of changes in the plant hydrogen production rate set-point or major operational disturbances (e.g., severe changes in ambient temperature or composition of the feedstock), and any adjustment to the optimized FSF distribution would cause the reformer to be at a suboptimal operating condition, which would decrease the reformer thermal efficiency and, therefore, lower the plant's efficiency. As a result, adjustments to the FSF distribution are not frequently made as noted in Kumar et al. (2016). Additionally, the FSF distribution is typically changed every three days in industry, which allows the furnace-balancing scheme to complete at least two iterations before implementing the new optimized input to the on-line reformer. Finally, it is important to note that ~90% of the computational time of each iteration of the furnace-balancing scheme is designated to the data generation process as noted in Section 3, and simulations of the reformer CFD models are carried out by ANSYS Fluent, which provides a flexible computing environment for parallel processing. Therefore, the computational time of each furnace-balancing iteration can be decreased with a more powerful computational resource (i.e., more computing nodes), which allows more iterations to be completed in the alloted time period.

3.1. Case study A

In this subsection, the performance of the furnace-balancing scheme is investigated under the assumption that the flow control system is fully functional (i.e., the furnace-balancing optimizer has 48 decision variables). The simulation results generated during the first six iterations of the furnace-balancing scheme are presented and discussed.

The evolution of the data-driven model is shown in Fig. 6, which indicates that the data-driven model progressively becomes a more accurate representation of the reformer CFD data with more iterations of the furnace-balancing scheme due to a larger reformer CFD database. Fig. 6 shows the predicted OTWT distributions generated by the data-driven model match well with those generated

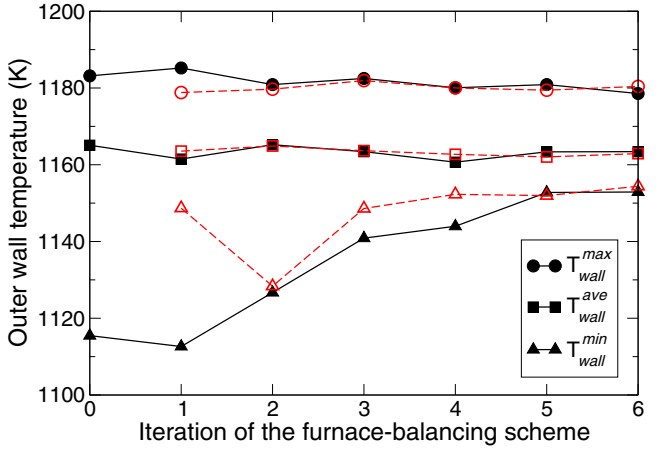

Fig. 6. Evolution of the maximum, average and minimum temperature values of the OTWT distribution at a distance 6.5 m away from the reforming tube inlets during the first 6 iterations of the furnace-balancing scheme, which are generated by the reformer CFD model (black symbols) and by the data-driven model (red symbols). (For interpretation of the references to color in this figure legend, the reader is referred to the web version of this article.)

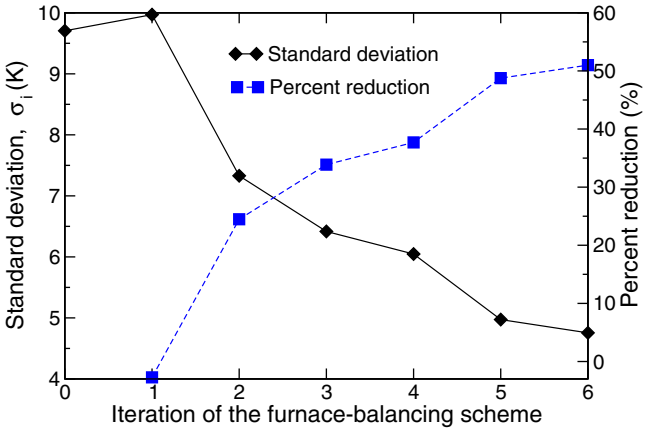

Fig. 7. Evolution of the standard deviation of the OTWT distribution at a distance 6.5 m away from the reforming tube inlets during the first 6 iterations of the furnace-balancing scheme, which are obtained from the reformer CFD model. The percent reduction in the magnitude of the standard deviation of the *i*th iteration with respect to the 0th iteration (i.e., $\frac{\sigma_i-\sigma_0}{\sigma_0}$) in the first 6 iterations is also shown. (For interpretation of the references to color in this figure legend, the reader is referred to the web version of this article.)

by the reformer CFD model with just five training data sets from the reformer CFD database, which validates our hypotheses of the impact of the furnace-side flow pattern on the OTWT distribution, the size of the cylindrical heating zone, the altered shape of the heating zone and the assumption that the radial average temperature of the *i*th reforming tube at a fixed distance away from the reforming tube inlet can be expressed as a linear combination of the FSF distribution.

Next, the evolution of the OTWT distribution at a distance 6.5 m away from the reforming tube inlets is shown in Figs. 6–8, which reveal that the reformer CFD model, in which the optimized FSF distribution is used as the boundary condition, has a less severe degree of nonuniformity in the OTWT distribution after the first iteration of the furnace-balancing scheme. Fig. 8 is created to allow data visualization (allowing the 336 reforming tubes in the reformer to be represented by a table consisting of 336 rectangular cells, of which each location in the table maps to a unique reforming tube in the reformer) so that the performance of the furnace-balancing scheme and the degree of nonuniformity of the OTWT distribution can be evaluated qualitatively at a glance (e.g., if Fig. 8 has a high number of red and green cells, the OTWT distribution is highly nonuniform). Fig. 8 shows that the OTWT distribution gradually becomes more uniform with more iterations of the furnace-balancing scheme. Specifically, by the 2nd iteration, the under-heated region near the reformer outlets in the OTWT distribution of the 0th iteration (i.e., the reformer CFD model of which the uniform FSF distribution is used as the boundary condition) is completely eliminated, by the 4th iteration the other noticeable under-heated region near the refractory back wall in the OTWT distribution of the 0th iteration is completely removed, and by the 6th iteration the severity of the two over-heated regions in the OTWT distribution of the 0th iteration is reduced. Figs. 6 and 7 are utilized to quantitatively evaluate the performance of the furnace-balancing scheme and the degree of nonuniformity of the OTWT distribution. From the 2nd iteration onward, Figs. 6 and 7 show that the temperature range and standard deviation of the OTWT distribution decrease compared to those of the 0th iteration. Specifically, at the 6th iteration of the furnace-balancing scheme, the temperature range and standard deviation of the OTWT distribution are reduced from 67.7 K and 9.7 K to 25.7 K and 4.8 K, respectively. The reduction in the standard deviation of the OTWT distribution due to the optimized FSF distribution with respect to the basis is 51%.

Finally, the evolution of the overall maximum outer wall temperature of the reforming tubes is shown in Fig. 9, which indicates that the reformer CFD model, in which the optimized FSF distribution (generated at any iteration of the furnace-balancing scheme) is used as the boundary condition, has a lower maximum outer reforming tube wall temperature compared to that of the 0th iteration. Specifically, at the 6th iteration of the furnace-balancing scheme, the overall maximum outer temperature of the reforming

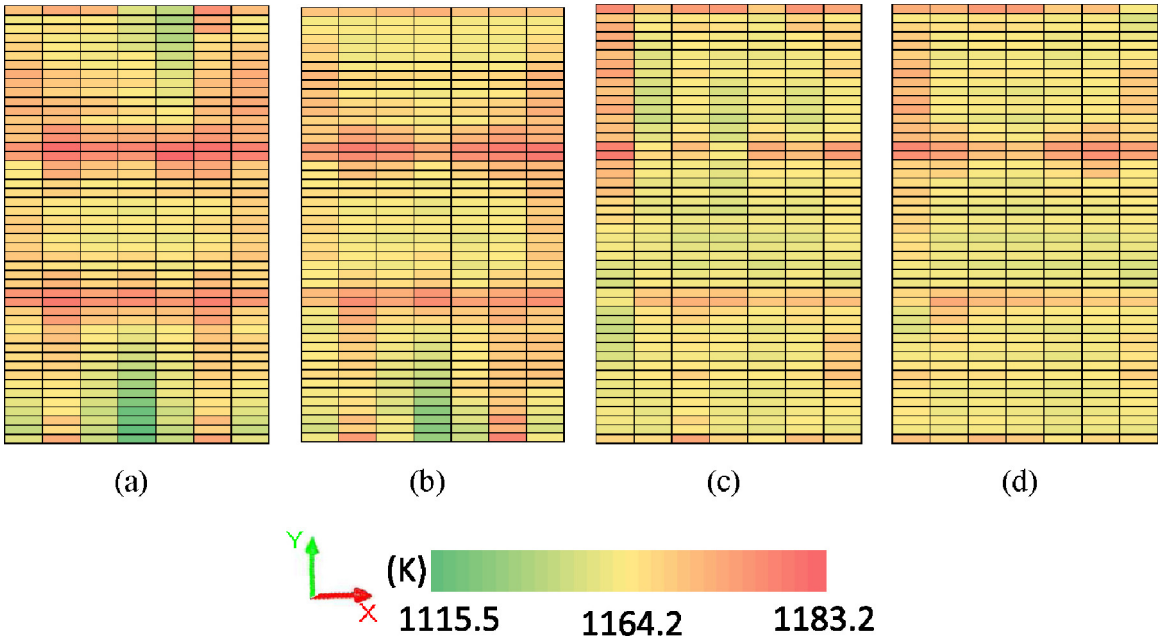

Fig. 8. Evolution of the OTWT distribution at a distance 6.5 m away from the reforming tube inlets during the first 6 iterations of the furnace-balancing scheme, which is obtained from the reformer CFD model, is displayed by comparing the OTWT distributions in the 0th (a), 2nd (b), 4th (c) and 6th (d) iterations. In Fig. 8, the top row of each subfigure corresponds to the reforming tubes that are the closest to the reformer outlets, and the bottom row of each subfigure corresponds to the reforming tubes that are the furthest away from the reformer outlets.

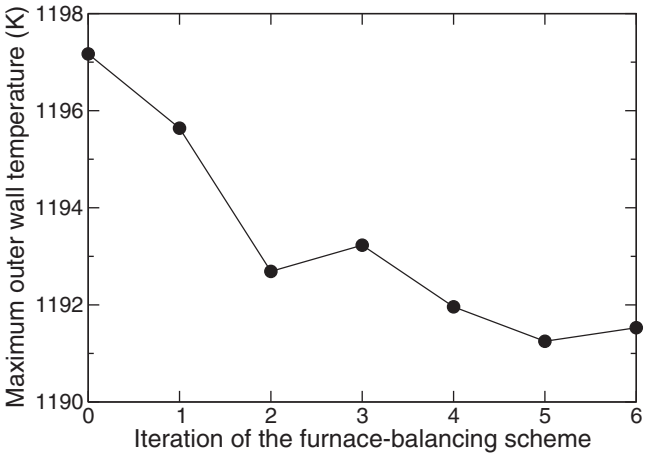

Fig. 9. Evolution of the overall maximum outer wall temperature along the reforming tube length among 336 reforming tubes in the reformer during the first 6 iterations of the furnace-balancing scheme, which are obtained from the reformer CFD model.

tubes is reduced from 1197.2 K to 1191.5 K (by 5.6 K). We would like to note that although the magnitude of the reduction in the overall maximum outer reforming tube wall temperature is much less than the overall average outer wall temperature of 1121.6 K, the contribution of our present work for industrial applications that strive to improve the thermal efficiency and service life of the reformer remains significant for the reason noted in Section 1. Due to the reduction in the overall maximum outer reforming tube wall temperature, the total FSF mass flow rate to the reformer can potentially be increased to achieve a higher operating temperature of the furnace-side flow without reducing the reformer service life, which leads to a lower rate of methane leakage (i.e., unreacted methane) and higher production rates of hydrogen and superheated steam. As a result, the thermal efficiency of the reformer is improved.

3.2. Case study B

In this subsection, the performance of the furnace-balancing scheme is analyzed when the flow control system is subjected to two different valve-related disturbances, which are categorized based on the number of defective valves. We consider the reformer from case study A after six iterations of the furnace balancing scheme have been executed with all valves fully functional. Though the termination checker of the furnace balancing scheme indicated that the balancing procedure could be terminated after the 6th iteration if no significant changes in the plant dynamics occurred, we assume that the valve-related disturbances occur after the 6th iteration of the furnace-balancing scheme has been executed and that the furnace-balancing scheme is therefore required to continue iterating to determine an optimized FSF distribution given the change in the valve availability. The predicted optimized valve position distribution produced by the furnace-balancing optimizer in the 6th iteration when there were no defective valves cannot be utilized because the valve positions of the defective valves cannot be adjusted to the optimized positions. Hence, the valve position distribution that is sent to the valve-position-to-flow-rate converter to generate the boundary conditions of the reformer CFD model is non-optimal. As a result, the OTWT distributions obtained by implementing the FSF distribution determined at the 6th iteration prior to the occurrence of the valve-related disturbances are expected to have a high degree of nonuniformity when implemented in a CFD model that accounts for the valve-related disturbances, and the furnace-balancing scheme is continued. We will impose two different valve-related disturbances after the 6th iteration and will refer to the iteration of the furnace-balancing scheme assuming the first type of valve-related disturbance occurs after the 6th iteration as the 7th iteration, and to the iteration of the furnace-balancing scheme assuming the second type of valve-related disturbance occurs after the 6th iteration as the 9th iteration (according to the above analysis, we expect significant OTWT distribution nonuniformity in both the 7th and the 9th iterations). In the re-balancing iterations of the furnace-balancing scheme (i.e., the 8th and 10th iterations), the text file documenting the status of the flow control system is updated, which notifies the furnace-balancing optimizer of the defective valves. Additionally, we simulate the two disturbances by assuming that the defective valves of the flow control system are arbitrarily selected, in which the corresponding stuck valve positions are modified from the optimized valve position by 5–30%. The simulation results generated in the 7th, 8th, 9th and 10th iterations of the furnace-balancing scheme are presented and discussed.

Table 3
OTWT distribution obtained from the reformer CFD model in the 6th iteration in which the optimized FSF distribution is used as the boundary condition.

Distance down reforming tubes (m)	T_{AVE} (K)	T_{Max} (K)	T_{Min} (K)	Standard deviation (K)
6.0	1160.1	1177.9	1148.9	5.5
6.5	1163.4	1178.6	1152.9	4.8
7.0	1166.6	1180.0	1155.1	4.3
8.0	1171.8	1185.4	1160.1	4.5
9.0	1177.0	1191.5	1162.8	5.0
10.0	1166.8	1184.1	1155.1	4.9
11.0	1162.2	1181.4	1151.8	5.3
12.0	1160.7	1180.9	1150.2	5.6

Table 4
OTWT distribution obtained from the reformer CFD model in the 7th iteration when the FSF distribution is altered by the single-valve disturbance.

Distance down reforming tubes (m)	T_{AVE} (K)	T_{Max} (K)	T_{Min} (K)	Standard deviation (K)
6.0	1158.2	1177.2	1112.4	10.0
6.5	1161.6	1178.3	1118.1	9.3
7.0	1164.9	1180.4	1124.7	8.6
8.0	1170.2	1187.4	1134.9	8.0
9.0	1175.5	1194.3	1142.6	7.9
10.0	1165.4	1186.2	1134.7	7.8
11.0	1160.9	1182.4	1132.2	7.7
12.0	1159.5	1181.1	1132.9	7.4

Table 5
OTWT distribution obtained from the reformer CFD model in the 8th iteration when the FSF distribution is reoptimized to counter the impact of the single-valve disturbance.

Distance down reforming tubes (m)	T_{AVE} (K)	T_{Max} (K)	T_{Min} (K)	Standard deviation (K)
6.0	1160.1	1175.7	1148.6	5.3
6.5	1163.3	1177.8	1153.7	4.5
7.0	1166.4	1179.9	1157.5	4.1
8.0	1171.5	1185.0	1159.6	4.3
9.0	1176.6	1190.7	1162.8	4.7
10.0	1166.4	1182.6	1154.9	4.7
11.0	1161.8	1178.9	1151.4	5.0
12.0	1160.3	1177.8	1147.2	5.3

Table 6
OTWT distribution obtained from the reformer CFD model in the 9th iteration when the FSF distribution is altered by the three-valve disturbance.

Distance down reforming tubes (m)	T_{AVE} (K)	T_{Max} (K)	T_{Min} (K)	Standard deviation (K)
6.0	1159.4	1180.3	1129.6	7.5
6.5	1162.9	1180.9	1135.4	6.7
7.0	1166.3	1181.4	1142.1	6.0
8.0	1171.7	1187.4	1151.5	5.6
9.0	1177.0	1193.1	1158.9	5.7
10.0	1166.8	1184.5	1151.9	5.8
11.0	1162.2	1181.2	1147.9	5.9
12.0	1160.7	1180.6	1146.9	6.0

In the case in which the reformer CFD model is subjected to a single-valve disturbance, a flow control valve is assumed to become defective. In particular, the valve regulating the FSF mass flow rates of the 48th and 49th inner-lane burners is chosen; and while the 6th iteration of the furnace-balancing scheme suggests that the optimized valve position is 97%, the stuck valve position is 70%. The CFD data generated by the reformer CFD model, in which the flow control system is under the influence of the single-valve disturbance, is used to analyze the degree of nonuniformity of the OTWT distributions in the high temperature regions along the reforming tube length. Comparing Table 4 with Table 3 reveals that the OTWT distributions expectedly become more nonuniform at the 7th iteration compared to the 6th iteration. Specifically, the temperature range and standard deviation of the OTWT distribution at the location 6.5 m away from the reforming tube inlets in the 7th iteration increase by 34.6 K and 4.6 K. The results suggest that the furnace-balancing scheme must be made aware of the constraint imposed by the single-valve disturbance to properly reoptimize the FSF distribution.

In the 8th iteration, as the text file documenting the status of the flow control system has been updated, the furnace-balancing optimizer is aware of the defective valve, which allows the number of decision variables to be reduced from 48 to 47 as discussed in Section 2.4. We note that the furnace-balancing optimizer is designed to handle a varying number of decision variables, and this ability of the furnace-balancing optimizer makes the furnace-balancing scheme especially appealing for industrial applications that are interested in control and automation. The CFD data generated by the reformer CFD model, in which the reoptimized FSF distribution is used as the boundary condition, is used to investigate the ability of the furnace-balancing scheme to compensate for the impact of the single-valve disturbance occurring in the flow control system.

Fig. 10 shows that the OTWT distribution at a distance 6.5 m away from the reforming tube inlets produced in the 8th iteration is more uniform than that produced in the 7th iteration. Specifically, the under-heated region near the reformer outlets in the OTWT distribution of the 7th iteration is completely resolved in the 8th iteration, and the severity of the over-heated region in the 7th iteration is significantly lessened in the 8th iteration. Additionally, the OTWT distribution in the 8th iteration shown in Fig. 10(b) resembles the optimized OTWT distribution in the 6th iteration shown in Fig. 8(d) even though the corresponding optimized valve position distributions are completely different as shown in Table 8. This is because the FSF distributions produced by these optimized valve position distributions in the 6th and 8th iterations are very similar. Moreover, Table 5 shows that the degree of nonuniformity in the OTWT distributions in the high temperature regions along the reforming tube length in the 8th iteration is reduced with respect to the corresponding quantities in the 7th iteration. Specifically, in the OTWT distribution at the location 6.5 m away from the

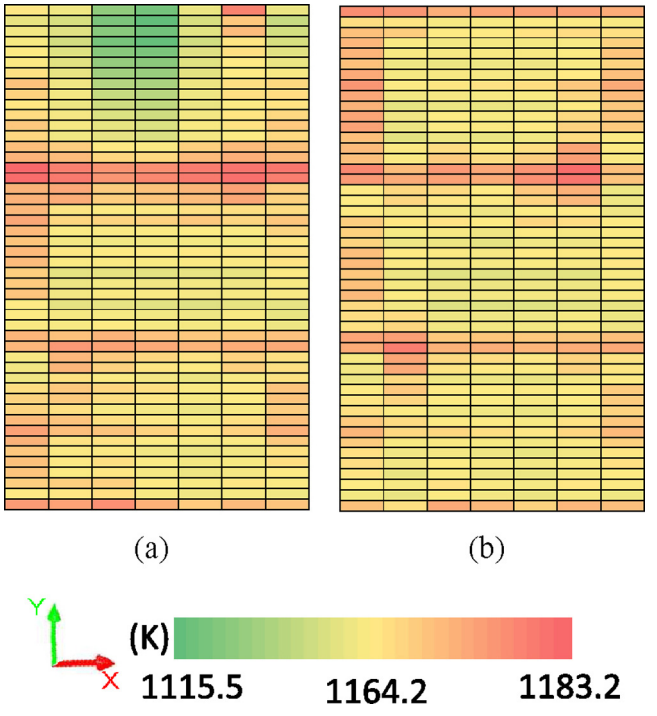

Fig. 10. Comparison between the OTWT distributions at a distance 6.5 m away from the reforming tube inlets generated from the 7th iteration when the FSF distribution is altered by the single-valve disturbance (a), and from the 8th iteration when the FSF distribution is reoptimized to counter the impact of the single-valve disturbance (b). In Fig. 10, the top row of each subfigure corresponds to the reforming tubes that are the closest to the reformer outlets, and the bottom row of each subfigure corresponds to the reforming tubes that are the furthest away from the reformer outlets.

Table 7
OTWT distribution obtained from the reformer CFD model in the 10th iteration when the FSF distribution is reoptimized to counter the impact of the three-valve disturbance.

Distance down reforming tubes (m)	T_{AVE} (K)	T_{Max} (K)	T_{Min} (K)	Standard deviation (K)
6.0	1159.1	1179.5	1137.0	6.6
6.5	1162.7	1180.1	1143.6	5.9
7.0	1166.2	1183.1	1151.3	5.3
8.0	1171.6	1188.6	1158.2	5.1
9.0	1177.0	1194.9	1165.0	5.2
10.0	1166.9	1187.9	1152.8	5.6
11.0	1162.4	1185.0	1148.1	5.9
12.0	1160.9	1184.3	1147.1	6.2

Table 8
Summary of the valve position distributions in the 0th, 6th, 7th, 8th, 9th and 10th iterations, in which the bold values represent the stuck positions of the defective valves due to the common valve-related disturbances.

V_i iteration	0th	6th	7th	8th	9th	10th
V_0	100	86	86	68	**70**	**70**
V_1	100	94	94	71	94	99
V_2	100	88	88	68	88	87
V_3	100	84	84	67	84	85
V_4	100	85	85	66	85	83
V_5	100	92	92	72	92	93
V_6	100	88	88	69	88	98
V_7	100	73	73	60	73	69
V_8	100	81	81	65	81	79
V_9	100	89	89	69	89	84
V_{10}	100	87	87	69	87	85
V_{11}	100	81	81	64	81	77
V_{12}	100	92	92	71	92	83
V_{13}	100	85	85	66	85	78
V_{14}	100	94	94	73	94	91
V_{15}	100	86	86	68	86	87
V_{16}	100	78	78	61	78	77
V_{17}	100	100	100	78	100	100
V_{18}	100	87	87	71	87	92
V_{19}	100	78	78	62	78	79
V_{20}	100	91	91	70	91	93
V_{21}	100	86	86	68	**80**	**80**
V_{22}	100	89	89	71	89	87
V_{23}	100	82	82	65	82	79
V_{24}	100	97	**70**	**70**	97	91
V_{25}	100	86	86	67	86	82
V_{26}	100	85	85	68	85	80
V_{27}	100	86	86	68	86	86
V_{28}	100	84	84	65	84	84
V_{29}	100	100	100	78	100	100
V_{30}	100	86	86	71	86	88
V_{31}	100	78	78	61	78	78
V_{32}	100	92	92	72	92	95
V_{33}	100	88	88	69	88	85
V_{34}	100	86	86	68	86	84
V_{35}	100	92	92	72	92	82
V_{36}	100	86	86	66	86	79
V_{37}	100	81	81	61	81	83
V_{38}	100	84	84	66	84	77
V_{39}	100	82	82	65	82	81
V_{40}	100	86	86	67	86	84
V_{41}	100	81	81	64	**90**	**90**
V_{42}	100	90	90	71	90	92
V_{43}	100	90	90	74	90	85
V_{44}	100	87	87	68	87	89
V_{45}	100	91	91	72	91	88
V_{46}	100	86	86	69	86	84
V_{47}	100	95	95	74	95	86

reforming tube inlets of the 8th iteration, the temperature range and standard deviation decrease to 24.1 K and 4.5 K. Therefore, the qualitative assessment (Fig. 10) and quantitative analysis (Table 5) of the degree of nonuniformity in the OTWT distribution between the 6th, 7th and 8th iterations indicates that the furnace-balancing scheme compensates for the impact of the single-valve disturbance occurring in the flow control system.

In the case when the reformer CFD model is subjected to a three-valve disturbance after the 6th iteration, three flow control valves become defective. In particular, the three valves which control the FSF mass flow rates of the 0th and 1st outer-lane burners and of the 42nd, 43rd, 82nd and 83rd inner-lane burners are selected, and the corresponding stuck valve positions are 70%, 80% and 90%, respectively, as opposed to their optimized valve positions of 86%, 87% and 81% in the 6th iteration of the furnace-balancing scheme. The only difference between the two disturbances occurring in the flow control system is the number of defective valves, and therefore, the analysis which is used to investigate the effects of the single-valve

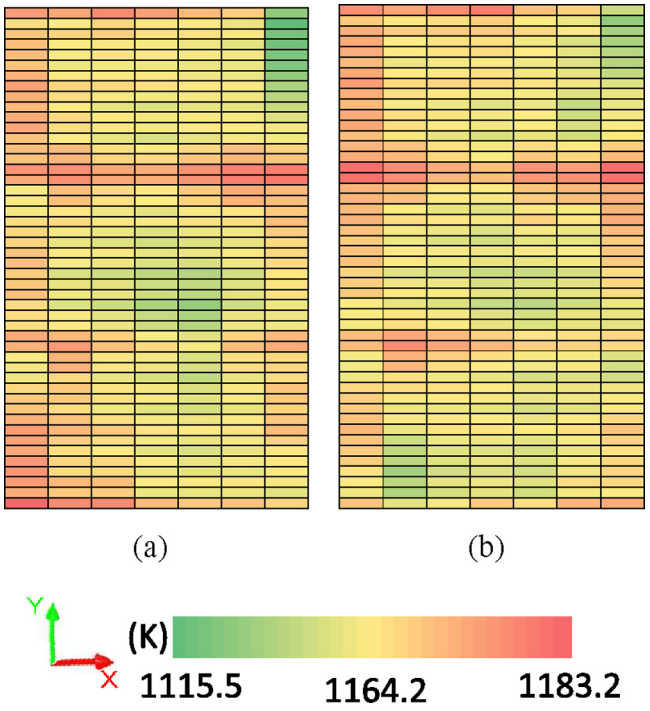

Fig. 11. Comparison between the OTWT distributions at a distance 6.5 m away from the reforming tube inlets generated from the 9th iteration when the FSF distribution is altered by the three-valve disturbance (a), and from the 10th iteration when the FSF distribution is reoptimized to counter the impact of the three-valve disturbance (b). In Fig. 11, the top row of each subfigure corresponds to the reforming tubes that are the closest to the reformer outlets, and the bottom row of each subfigure corresponds to the reforming tubes that are the furthest away from the reformer outlets.

disturbance on the degree of nonuniformity in OTWT distributions along the reforming tube length and the ability of the furnace-balancing scheme to compensate for the constraint imposed by the single-valve disturbance during the search for the reoptimized FSF distribution is also utilized.

The quantitative assessment of the effects of the three-valve disturbance on OTWT distributions in the high temperature region of the reforming tube length is presented in Table 6, which shows that the OTWT distributions of the 9th iteration are more nonuniform compared to the corresponding ones in the 6th iteration; and specifically, the temperature range and standard deviation of the OTWT distribution at the location 6.5 m away from the reforming tube inlets increase by 19.9 K and 1.9 K, respectively. Subsequently, the information of the three-valve disturbance is utilized to update the text file documenting the status of the flow control system in the 10th iteration, which notifies the furnace-balancing optimizer of the three defective valves and allows the number of decision variables to be reduced from 48 to 45. The CFD data generated by the reformer CFD model, in which the reoptimized FSF distribution is used as the boundary condition, is used to create Fig. 11 and Table 7 to investigate the ability of the furnace-balancing scheme to compensate for the impact of the three-valve disturbance. Specifically, Fig. 11 shows that the OTWT distribution produced in the 10th iteration is more uniform than that produced in the 9th iteration as the over-heated region near the left corner of the refractory back wall in the OTWT distribution of the 9th iteration is completely resolved in the 10th iteration, and the severity of the under-heated region near the reformer outlets in the 9th iteration is significantly lessened in the 10th iteration. Moreover, Table 7 shows that the degree of nonuniformity in most of the OTWT distributions in the high temperature regions along the reforming tube length in the 10th iteration is reduced compared to those in the 9th iteration, and specifically, the temperature range and standard deviation in the OTWT distribution at the location 6.5 m away from the reforming tube inlets decrease to 36.5 K and 5.9 K, respectively. Although the 10th iteration appears to be able to compensate for the impacts of the three-valve disturbance, which are observed in the 9th iteration, the OTWT distribution in the 10th iteration shown in Fig. 11(b) appears to have a higher degree of nonuniformity than the optimized OTWT distribution in the 6th iteration shown in Fig. 8(d). Therefore, the qualitative assessment (Fig. 11) and quantitative analysis (Table 7) of the degree of nonuniformity in the OTWT distribution between the 6th, 9th and 10th iterations indicates that the furnace-balancing scheme can compensate for the impact of the three-valve disturbance occurring in the flow distribution system.

4. Conclusion

In this work, we developed a robust model-based furnace-balancing scheme that can reduce the degree of nonuniformity in OTWT distributions along the reforming tubes inside the furnace of a steam methane reformer. To this end, we adopted a high fidelity reformer CFD model created in our previous work and developed a model identification process based on the effects of thermal radiation, the furnace-side flow pattern, reformer CFD data and the least squares regression method to approximate the relationship between the OTWT distribution and the FSF distribution. Then, we introduced the model-based furnace-balancing optimizer that accounts for typical industrial operational constraints and physical constraints on the flow control valves while searching for an optimal FSF distribution based on the data-driven model. The CFD data showed that the optimized FSF distribution created by the proposed furnace-balancing scheme allowed the degree of nonuniformity of OTWT distributions in the high temperature region of the reforming tubes and the overall maximum outer wall temperature to be reduced compared to the case in which a uniform FSF distribution was used. This result demonstrated that the proposed furnace-balancing scheme allowed the spatial distribution of the furnace-side temperature inside the combustion chamber to also become more uniform, which was expected to enhance the radiative heat transfer efficiency in the reformer. We also demonstrated the effectiveness of the furnace-balancing scheme in reducing the degree of nonuniformity of OTWT distributions in the presence of defects of the valves regulating the amount of furnace-side feed to the burners. The proposed balancing scheme allows taking advantage of the reduction in the overall maximum outer reforming tube wall temperature and the more uniform OTWT distributions to increase the total FSF mass flow rate to the burners, thereby increasing hydrogen production and extending reforming tube lifetime.

Acknowledgement

Financial support from the US Department of Energy is gratefully acknowledged.

References

ANSYS Inc., 2013. ANSYS Fluent Theory Guide 15.0.
Bane, S.P.M., Ziegler, J.L., Shepherd, J.E., 2010. Development of One-Step Chemistry Models for Flame and Ignition Simulations. Technical Report. GALCIT Report GALCITFM:2010.002.
Crose, M., Kwon, J.S.I., Tran, A., Christofides, P.D., 2017. Multiscale modeling and run-to-run control of PECVD of thin film solar cells. Renew. Energy 100, 129–140.
Dunn, A., Yustos, J., Mujtaba, I., 2002. Modelling and simulation of a top-fired primary steam reformer using gPROMS. Dev. Chem. Eng. Miner. Process. 10, 77–87.
Ewan, B., Allen, R., 2005. A figure of merit assessment of the routes to hydrogen. Int. J. Hydrogen Energy 30, 809–819.

Ferreira-Aparicio, P., Benito, M., Sanz, J., 2005. New trends in reforming technologies: from hydrogen industrial plants to multifuel microreformers. Catal. Rev. 47, 491–588.
Kroschwitz, J.I., Howe-Grant, M. (Eds.), 1999. Kirk–Othmer Encyclopedia of Chemical Technology. John Wiley and Sons Inc., New York, NY.
Kumar, A., Baldea, M., Edgar, T.F., 2016. Real-time optimization of an industrial steam-methane reformer under distributed sensing. Control Eng. Pract. 54, 140–153.
Kumar, A., Baldea, M., Edgar, T.F., Ezekoye, O.A., 2015. Smart manufacturing approach for efficient operation of industrial steam-methane reformers. Ind. Eng. Chem. Res. 54, 4360–4370.
Lao, L., Aguirre, A., Tran, A., Wu, Z., Durand, H., Christofides, P.D., 2016. CFD modeling and control of a steam methane reforming reactor. Chem. Eng. Sci. 148, 78–92.
Latham, D., 2008. Mathematical Modeling of an Industrial Steam Methane Reformer. Masters Thesis. Queen's University.
Lee, J.S., Seo, J., Kim, H.Y., Chung, J.T., Yoon, S.S., 2013. Effects of combustion parameters on reforming performance of a steam-methane reformer. Fuel 111, 461–471.
Maximov, A., 2012. Thesis for the Degree of Doctor of Science: Theoretical Analysis and Numerical Simulation of Spectral Radiative Properties of Combustion Gases in Oxy/Air-fired Combustion Systems. Lappeenranta University of Technology.
Nicol, D.G., 1995. A Chemical Kinetic and Numerical Study of NO_x and Pollutant Formation in Low-Emission Combustion. Ph.D. Thesis. University of Washington.
Olivieri, A., Vegliò, F., 2008. Process simulation of natural gas steam reforming: fuel distribution optimisation in the furnace. Fuel Process. Technol. 89, 622–632.
Oprins, A.J.M., Heynderickx, G.J., 2003. Calculation of three-dimensional flow and pressure fields in cracking furnaces. Chem. Eng. Sci. 58, 4883–4893.
Pantoleontos, G., Kikkinides, E.S., Georgiadis, M.C., 2012. A heterogeneous dynamic model for the simulation and optimisation of the steam methane reforming reactor. Int. J. Hydrogen Energy 37, 16346–16358.
Tran, A., Aguirre, A., Durand, H., Crose, M., Christofides, P.D., 2017. CFD modeling of an industrial-scale steam methane reforming furnace. Chem. Eng. Sci (submitted for publication).
Vuthaluru, R., Vuthaluru, H., 2006. Modelling of a wall fired furnace for different operating conditions using FLUENT. Fuel Process. Technol. 87, 633–639.
Wächter, A., Biegler, L.T., 2006. On the implementation of an interior-point filter line-search algorithm for large-scale nonlinear programming. Math. Program. 106, 25–57.
Xu, J., Froment, G.F., 1989. Methane steam reforming, methanation and water-gas shift. I. Intrinsic kinetics. AIChE J. 35, 88–96.
Zheng, D., Wu, B., Fleitz, J., Trajkovski, R., Zhou, C.Q.,2010. CFD simulation of a hydrogen reformer furnace. In: Proceedings of the 14th International Heat Transfer Conference. American Society of Mechanical Engineers, pp. 233–244.